Check for updates

Characteristics of poly-silicate aluminum sulfate prepared by sol method and its application in Congo red dye wastewater treatment†

Yunlong Zhao,[a] Yajie Zheng, [iD] *[a] Yinglin Peng,[b] Hanbing He[a] and Zhaoming Sun[a]

A novel method for synthesizing poly-silicate aluminum sulfate coagulant (PSAS) using a silica-alumina sol was reported. Herein, two modalities ($nSiO_2/nNa_2O$: 1.11 and 3.27) of self-made water glasses were used as the silica source for synthesizing the sol precursor. Then, the $PSAS_{1.11}$ and $PSAS_{3.27}$ with different basicity were obtained by controlling the Al molar ratio of precursor to aluminum sulfate. The results showed that the $PSAS_{1.11}$ coagulant prepared with low modulus water glass (LMWS, 1.11) has low turbidity and good stability. Using low modulus water glass, the effect of the Al molar ratio of precursor to aluminum sulfate on the basicity and stability of $PSAS_{1.11}$ with Al/Si of 20 and the effect of the molar ratio of aluminum to silicon on the basicity and stability of $PSAS_{1.11}$ were studied, respectively. Based on XRD and Fourier infrared (FTIR) characterization of the sol precursor and $PSAS_{1.11}$, the synthesis mechanism of PSAS by the silica-alumina sol method was discussed. Al species distribution of $PSAS_{1.11}$ was determined using the Al-Ferron timed spectrophotometric method. Moreover, the performance of $PSAS_{1.11}$ coagulant was examined, regarding its efficiency towards color removal of Congo red. The results showed that $PSAS_{1.11}$ coagulant with Al/Si of 20 and Al molar ratio of 1/12 exhibits excellent performance, and the color removal rate reached 98.6% at an initial pH of 11 and coagulant dosage of 40 mg L^{-1} (Al mg L^{-1}). Finally, the PSAS coagulant mechanism was discussed in detail through infrared characterization, ^{27}Al NMR, Raman, morphology and mapping of the flocs.

1. Introduction

Synthetic dyes are a necessity in various significant industries such as the paper, fiber, leather as well as textile industries for their colour-giving properties.[1] Currently, more than 7000 types of synthetic dyes have been reported. It is estimated that 7×10^5 to 1×10^6 tonnes of various colourings are manufactured from about 100 000 commercially accessible dyes each year.[2,3] However, during the production and use of dyes, approximately 10% of the dyes are released into the ecosystem as wastewater. Synthetic dyes, as the common pollutant in wastewater, are often toxic and carcinogenic, posing a great threat to the survival of terrestrial and marine life. Dyeing wastewater is characterized by deep color, high toxicity, high chemical oxygen demand (COD) and biochemical oxygen demand (BOD) values, complex composition, large discharge, wide distribution, and difficult degradation.[4,5] Therefore, treatment of dye wastewater has been widely concerned. Several methods include biological approach, sedimentation,

adsorption, oxidation, coagulation and flocculation (CF) have been reported.[6–9] Biological methods are effective in reducing the chemical oxygen demand (COD) required for wastewater treatment, however, non-completely decolorize. Oxidation methods are complex, and it often needs to be used in combination with other methods. The adsorption method is difficult to apply in industry because of the difficulty of regenerating the adsorbent and the long adsorption time. CF methods are widely recognized and widely used because of its simple operation, large processing capacity and low investment cost.[10,11]

For coagulation process, the coagulant with excellent performance is the core technology and research concerns. With the improvement of human living standards, conventional coagulation, such as aluminum and iron salts, can no longer meet the demand due to their high dosage and high residual metal concentration. They are gradually replaced by organic and inorganic polymer coagulants developed in recent years. Organic polymer coagulant is very variety and excellent performance. However, due to the high price and non-completely eliminating toxicity, it is mainly used as coagulation auxiliaries. Inorganic polymer flocculants have stronger electrical neutralization and net flutter bridging functions than traditional coagulation. They are also rapidly developed and used because of their cost-effective.[12,13] The use of iron-base inorganic polymer coagulants is far inferior to that of aluminum

[a]School of Metallurgy and Environment, Central South University, Changsha 410083, China. E-mail: zyj@csu.edu.cn

[b]School of Materials and Chemical Engineering, Hunan City University, Yiyang 413099, China

† Electronic supplementary information (ESI) available. See DOI: 10.1039/d1ra06343j

inorganic polymer coagulants owing to low adjustable basicity and deep color of wastewater treated. So, aluminum inorganic polymer coagulants, such as polymeric aluminum chloride (PAC), poly-silicate aluminum chloride (PSAC), poly-silicate aluminum sulfate (PSAS) and poly-silicate aluminum ferric sulfate (PSAF) *etc.*, have good performance in the coagulation of various wastewaters. Among of Si-containing coagulants, the introduction of silicic acid can enhance the coagulation bridging ability and complement the deficiency of original molecular weight and particle size. So, those coagulation has received particular attention.[14]

Usually, coexisting anions in the hydrolyzed aluminum solution are an important factor affecting the coagulation effect of aluminum-based coagulants, while affect the Al species distribution and structure of the coagulants. Coordination affinity of OH^- to Al^{3+} is far greater than other anions such as Cl^-, NO_3^- and SO_4^{2-}. The order of coordination affinity between anion and Al^{3+} is: $SO_4^{2-} > Cl^- > NO_3^-$. Therefore, compared with PSAC, PSAS has a lower content of Al in the form of monomer or dimer (*i.e.*, Al_a), while the content of polymers (Al_b) and $Al(OH)_3$–solid (Al_c) is higher.[15-18] Meanwhile, the source of aluminum sulfate is more extensive than that of aluminum chloride, and it has reliable industrial production and is cheaper. Therefore, PSAS has higher research value than PSAC. Qiu *et al.*, reported that banknote printing wastewater was treated using poly-silicate ferro-aluminum sulfate (PSFA). The maximal colour removal efficiency of 98% and COD removal efficiency of 85% could be achieved at the optimal dosage of 30.33 g L^{-1}.[19] The treatment of arsenic-containing wastewater by using PSFA and PSAS coagulants was reported by Li *et al.* The removal efficiency of arsenic was 98% and 93% respectively, when the molar ratio of $(Fe^{3+} + Al^{3+})/SiO_2$ was 2 : 1 and 1 : 1 using PSFA coagulant.[20] In another study, polysilicate aluminum magnesium (PSAM) and cationic polyacrylamide (cPAM) were stepwise used for drinking water treatment. Under suitable conditions, the removal efficiency was over 98% for turbidity and color, respectively.[21] To the best of the author's limited knowledge, the synthesis of PSAS is mainly divided into compound method and copolymerization two methods.[12,22] The treatment of oil-contaminated water using the poly-silicate aluminum ferric sulfate prepared by compound method was reported by You *et al.*[23] Compound method needs to obtain a poly-silicate acid solution in advance. In the compounding method, poly-silicate acid was prepared and used immediately to prevent the solution from gelation and thus loss of coagulation performance, its polymerization degree is difficult to control, as well insufficient combination of silicon and aluminum.[24] Copolymerization method firstly mix sodium silicate and aluminum sulfate, and then alkalize and polymerize by using alkaline substances such as sodium aluminate, sodium carbonate or sodium hydroxide to obtain PSAS. Although the copolymerization method can avoid this phenomenon, silicon is easy to precipitate during the alkalization polymerization process. Moreover, the polymerization process requires strong agitation *i.e.* high speed shear force.[12] Therefore, to overcome the drawbacks of the above methods, this work proposes a sol precursor method for the preparation of PSAS.

Inspired by the preparation of zeolite from silica alumina sol, this research proposes a novel method for preparing PSAS from silica alumina sol. Herein, two modulus water glass extracted from bauxite reaction residue was used as silica source[25] and mixed it with sodium aluminate to prepare sol precursor. Then, the $PSAS_{1.11}$ and $PSAS_{3.27}$ with different basicity were obtained by controlling Al molar ratio of precursor to aluminum sulfate. Later, a detailed study of synthesis of $PSAS_{1.11}$ by using low modulus water glass was carried out, including the Al molar ratio of precursor to aluminum sulfate and the silica–aluminum ratio in $PSAS_{1.11}$. The process and mechanism of the preparation of $PSAS_{1.11}$ are discussed in detail based on the XRD and FTIR characterization of the precursor and PSAS. Moreover, the removal mechanism of Congo red was discussed by Al species analysis and flocs (combination of Congo red and $PSAS_{1.11}$ coagulant) infrared analysis.

2. Materials and methods

2.1 Preparation of poly-silicate aluminum sulfate by sol method

2.1.1 Preparation of sol precursor. Sodium aluminate (chemically pure, $Al_2O_3 \geq 41.0\%$, Sinopharm Chemical Reagent Co., Ltd) was dissolved in quantitative deionized water, and then added a small amount of stabilizer. The above mixed liquid was boiled and cooled to room temperature to obtain a clarified sodium aluminate solution (1 mol L^{-1}). Then, two kinds of modulus water glass (modulus 3.27 and SiO_2 content 27.3 wt%, modulus 1.11 and SiO_2 content 6.5 wt%) are diluted to 5 wt% solution (silica concentration), respectively. Silica aluminum sol precursors were obtained by mixing sodium aluminate solution and water glass. They are labeled as $precursor_{1.11}$ and $precursor_{3.27}$, respectively.

2.1.2 Preparation of PSAS coagulant. Here, a brief process of preparation PSAS using sol precursor is shown in Fig. 1. First, aluminum sulfate octahydrate (analytical purity $\geq$ 99.0%, Sinopharm Chemical Reagent Co., Ltd) was dissolved in deionized water to prepare 0.8 mol L^{-1} $Al_2(SO)_4$ solution. Second, at a stirring rate of 500 rpm, different doses of precursors were slowly added to the aluminum sulfate solution to form a translucent suspension, and then it was stirred for 0.5 h at room temperature. The suspension was heated to 75 °C for digestion. Finally, after polymerization for 2 h and cooling to room temperature, the PSAS solutions were obtained. In the above preparation of PSAS, the effect of aluminum molar ratio
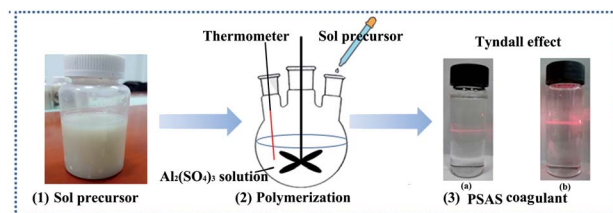

Fig. 1 PSAS preparation process diagram.

of precursor to aluminum sulfate on coagulation stability was investigated by using two precursors (1.11 and 3.27), marked as $PSAS_{1.11}$ and $PSAS_{3.27}$. Due to the better stability of $PSAS_{1.11}$ coagulant synthesized by low modulus water glass, the $precursor_{1.11}$ was used to study the effect of the Al molar ratio of precursor to aluminum sulfate on the stability and basicity of $PSAS_{1.11}$ prepared with Al/Si of 20. Liquid PSAS was vacuum-dried at 50 °C, and then grounding to powder samples for structural analysis.

2.2 Analysis and methods

2.2.1 Characterization of poly-silicate aluminum sulfate solid powder. Coagulant solid powder was determined by using D/MAX-RB X-ray diffractometer (Rigaku, Japan) with Cu K-radiation in the 2θ range of 10–80° at a scan rate of $10°$ min^{-1}. The morphology of the precursor, coagulants and combination of dye and coagulant were examined by JSM-6360LV scanning electron microscope (SEM), respectively. Infrared spectra of precursor sol, coagulants and combination of dye and coagulant were measured *via* a Fourier-transform infrared (FTIR) spectrometer (Nissan Hitachi, 270-30) by using the potassium bromide pellet method. ^{27}Al NMR spectra were taken under the resonance frequency of 10 kHz.

2.2.2 Ferron method to test Al species distribution. Aluminum species distribution in PSAS was measured by using Al-Ferron timed spectrophotometric method,[26] which is based on the different reaction time of aluminum species with the Ferron reagent (8-hydroxyl-7-iodoquinoline-5-sulphonic acid). Because of complexes of Al with Ferron reagent have maximum absorption at a wavelength of 370 nm, hence, different species of aluminum (*i.e.* Al_a – monomers, Al_b – polymers and Al_c – $Al(OH)_3$ or solids) would be calculated *via* absorbance measurements at this wavelength. The absorbance A_a and A_b of Al_a and Al_b components are converted to the corresponding concentrations of C_a and C_b according to the aluminum standard curve relationship eqn (1)–(3). Then:

$$Al_a = C_a/C_T \times 100\% \qquad (1)$$

$$Al_b = C_b/C_T \times 100\% \qquad (2)$$

$$Al_c = 1 - (Al_a + Al_b) \qquad (3)$$

where C_T is the total aluminum concentration of the sample, C_T in the PSAS was measured by using 2 mol L^{-1} nitric acids to decompose the polymer into monomers.

2.2.3 Jar test and calculation of the color removal efficiency. Synthetic dyeing wastewater was prepared by adding designated amounts of Congo red in deionized water. The absorbance fitting curve of Congo red dye standard solution is shown in Fig. S3.† The absorbance of Congo red at λ_{max} varies linearly with the concentration. Therefore, the concentration change of the dye can calculate based on the absorbance. The performance testing of coagulant was carried out with 100 mg L^{-1} simulated dyeing wastewater. Comparability and reliability of each data set are ensured by the use of six league electric blenders. The initial pH of dyeing wastewater was

properly adjusted by using H_2SO_4 or NaOH solutions of appropriate concentrations in the range of 1–0.01 mol L^{-1}. In briefly, the coagulation process was described. 250 mL dye wastewater was poured into 500 mL drying beaker and placed into the stirring device. After adding the PSAS, the dye waste-water was stirred rapidly at 300 rpm for 2 min, and then slowly stirred at 60 rpm for 10 min. The water samples were collected at 2 cm under the surface of water after settling for 20 min, and further measured the final absorbance. Color removal efficiency ($\eta\%$) would allow the calculation according to the eqn (4):

$$\eta\% = (A_0 - A_t)/A_0 \times 100 \qquad (4)$$

Where A_0 is the initial absorbance of the dyeing wastewater, A_t is the absorbance of supernatant at the corresponding settling time (t) after the coagulation run. It should be noted that the dosage of coagulant was calculated as mg Al per L for PSAS coagulants.

3. Results and discussion

3.1 The structure and morphology of the precursor

XRD pattern of the sol $precursor_{1.11}$ solid powder is shown in Fig. 2(a). The precursor has no obvious diffraction peaks, which indicate that the $precursors_{1.11}$ is no long-range crystalline order. In the sol formed by the combination of sodium aluminate and sodium silicate, silicon is preferentially combined with silicon or aluminum to form a Si–O–Si or Al–O–Si tetrahedral structure. The colloids formed during this process are almost the same as those formed before zeolite transcrystallization, so the colloidal particles show no long-range crystalline order structure.[27] Meanwhile, it can be seen from Fig. 2(c) that the precursor is formed by agglomeration of regular-shaped particles. Fig. 2(d) shows the energy spectra of the relevant elements in the precursors. Oxygen is the most abundant element in the precursor. In addition, the aluminum
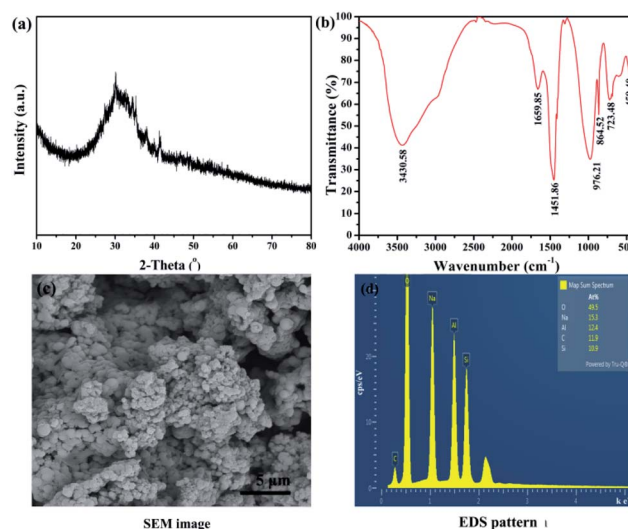

Fig. 2 Precursor characterization; (a) XRD diffraction pattern, (b) FTIR spectra and (c) SEM images (d) EDS pattern.

content is greater than that of silicon, which facilitates the adequate combination of aluminum and silicon. PSAS coagulants prepared by using this precursor may have good performance.

Fig. 2(b) presents the FT-IR spectra of sol precursor$_{1.11}$. The peak at 3430.58 cm^{-1} can be attributed to the intermolecular association of the stretching vibration of –OH.[28] The stronger absorption band located at 976 cm^{-1} is associated with aluminosilicate skeleton vibration.[27] This indicates that sodium silicate and sodium aluminate do form soluble silica–aluminum colloids. The characteristic peak at 1655.85 cm^{-1} is the stretching vibration of water absorbed. The peak at about 948 cm^{-1} corresponds to the symmetric stretching vibrational structure of Si–O–Al. The peaks at 603–605 and 459–460 cm^{-1} are associated with the single bond vibrations of Si–O and Al–O, respectively. Two peaks at 723.48 cm^{-1} and 632 cm^{-1} are attributed to the antisymmetric bending and stretching vibrations of Al–OH, respectively.

3.2 Stability and basicity of PSAS coagulants

3.2.1 Effects of the Al molar ratio of precursor to aluminum sulfate on the basicity and stability of PSAS. Fig. 3(a) shows the influence of the Al molar ratio of precursor to aluminum sulfate on the PSAS coagulant basicity by using two modalities of water glass as silica source. The basicity of PSAS increases significantly with the increasing Al molar ratio. In the case that the precursor does not contain sodium aluminate, the basicity of coagulant prepared with high modulus water glass is higher than that of coagulant prepared with low modulus water glass. The basicity of the PSAS product prepared using a water glass with a modulus of 3.27 was 7.9%, while the basicity of the PSAS prepared using a water glass with a modulus of 1.11 was 13.7%. The reason for this result is the high alkali content in the low

modulus water glass. However, when using precursors prepared from sodium aluminate containing, it is interesting that the basicity of PSAS$_{3.27}$ coagulants is higher than that of PSAS$_{1.11}$. This is attributed to the fact that low modulus water glass has more mononuclear silicon. The NaAlO$_2$ available in the precursor for controlling the basicity of PSAS is reduced due to the sufficient combination of aluminum and silicon. So its basicity is slightly lower than PSAS$_{3.27}$ coagulant. Compared to PSAS$_{3.27}$, PSAS$_{1.11}$ is less prone to gelation and has a smaller molecular weight. The variation of turbidity is consistent with this conclusion. Therefore, it is advisable to use low modulus water glass to synthesize PSAS coagulant.

As shown in Fig. 3(b), the turbidity of PSAS coagulant increases with the increase in basicity.[29] Especially, the turbidity increases significantly when the high modulus water glass is used. In terms of amorphous silica dissolved in strong alkali to form water glass, usually, there are three important areas in the amorphous silicon concentration pH diagram: (1) the insoluble domain is the precipitation zone of amorphous silicon; (2) the multimeric domain where silicon polyanions are stable; and (3) the monomeric domain where mononuclear Si species [Si(OH)$_4$, SiO(OH)$_3^-$, and SiO$_2$(OH)$_2^{2-}$] prevail thermodynamically.[30] Silica is mainly stabilized in water glasses (3.27) as polyanions and mononuclear. In contrast, a small amount of Si polyions is present in the low modulus water glass.

Table 1 presents the physical properties of PSAS coagulant. PSAS$_{3.27}$ coagulant is very unstable and usually shows significant gelation after 2–3 days of storage at ambient temperature. Due to the poor stability, we did not consider subsequent dye performance tests on this material. However, the obtained PSAS$_{1.11}$ coagulant is a clear colloidal solution with good stability, and its stability is enhanced significantly. Meanwhile, the PSAS$_{1.11}$ coagulant solution has Tyndall effect as showing in Fig. S1.†

Above-mentioned PSAS$_{1.11}$, its basicity and ratio of Al/Si increase with the increase in the Al molar ratio of precursor to aluminum sulfate. Therefore, it is difficult to determine whether it is the aluminum to silicon ratio or the salinity that affects the performance of PSAS$_{1.11}$ coagulant. Therefore, PSAS$_{1.11}$ coagulants with aluminum–silica ratio of 20 were synthesized. Variation of coagulant basicity is shown in Fig. 2(c). It can be seen from Fig. 3(c) that the basicity of PSAS$_{1.11}$ coagulant is linearly increasing in relation to the aluminum
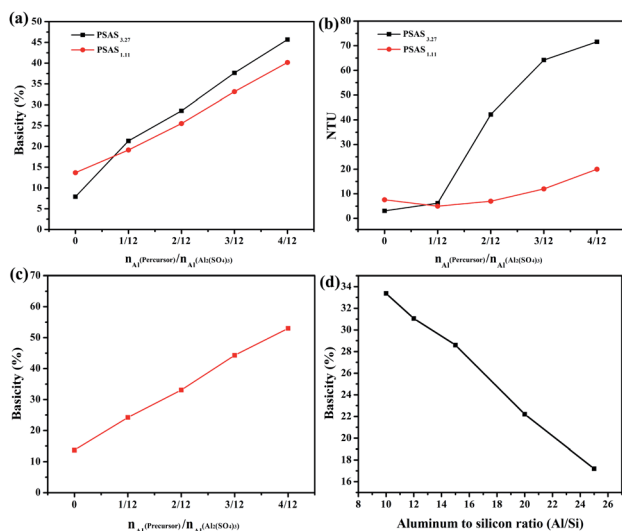

Fig. 3 Effect of the Al molar ratio on the PSAS basicity (a) and on the PSAS solution turbidity (b) and (c) effect of the Al molar ratio on the basicity of PSAS$_{1.11}$ (Al/Si of 20); (d) effect of the ratio of the ratio of aluminum to silica on the basicity of PSAS$_{1.11}$ (Al molar ratio of 1/12).

Table 1 Influence of the Al molar ratio of precursor to aluminum sulfate on the pH and stability of the synthesized PSAS

$n_{Al(precursor)}/n_{Al(aluminum\ sulfate)}$	0	1/12	2/12	3/12	4/12
Al/Si(PSAS$_{3.27}$)	20	21.6	23.3	24.8	26.7
Al/Si(PSAS$_{1.11}$)	20	21.6	23.3	24.8	26.7
Al/Si(PSAS$_{1.11}$)	20	20	20	20	20
Gel (day) (PSAS$_{3.27}$)	30	2	3	3	3
Gel (day) (PSAS$_{1.11}$)	60	23	34	Ungelled	Ungelled
Gel (day) (PSAS$_{1.11}$, Al/Si of 20)	60	20	75	Ungelled	Ungelled
pH value (PSAS$_{3.27}$)	2.53	3.15	3.16	3.19	3.25
pH value (PSAS$_{1.11}$)	2.86	3.28	3.33	3.34	3.36
pH value (PSAS$_{1.11}$, Al/Si of 20)	2.86	3.29	3.38	3.45	3.47

molar ratio of the precursor to aluminum sulfate. Therefore, the PSAS with different basicity prepared by precursor has obvious advantages, example controllable basicity. The physical properties of PSAS$_{1.11}$ with aluminum to silica ratio of 20 are shown in Table 1.

3.2.2 Influence of the ratio of silica and aluminum in PSAS$_{1.11}$ coagulant on the basicity and stability. From the subsequent performance experiments, it can be seen that the aluminum to silicon ratio as well as the basicity have different degrees of influence on the coagulant performance. Moreover, the synthesized PSAS$_{1.11}$ with Al molar ratio of 1/12 exhibits excellent performance in subsequent performance experiments. And the performance of PSAS$_{1.11}$ with an Al/Si of 20 is slightly higher than that of PSAS$_{1.11}$ with an Al/Si ratio of 21.6, indicating that a proper reduction of the Al/Si ratio in the coagulant is beneficial to improve the performance of the coagulant. Factors affecting the performance of the coagulant will be discussed in detail later. So, under Al molar ratio of 12 conditions, the PSAS$_{1.11}$ coagulants with different Al/Si were further synthesized. The effect of aluminum–silicon ratio on the basicity of PSAS$_{1.11}$ is shown in Fig. 3(d).

The pH and gel time data for PSAS$_{1.11}$ solution are given in Table 2. The results showed that the pH value and basicity of PSAS$_{1.11}$ increased with the decrease of aluminum to silicon. Increase of PSAS basicity means that hydroxyl groups are consumed during the polymerization process of aluminum sulfate. If the hydroxyl group is provided by water causing the coagulant basicity increases, the pH of the solution will inevitably decrease. However, the interpretation is contrary to the experimental results. Since the precursors have the same Al content, the increased alkalinity of the coagulant could only be caused by the water glass.

3.3 Analysis of the structure and morphology of PSAS coagulant

3.3.1 XRD analysis of PSAS$_{1.11}$ powder. The XRD pattern of PSAS$_{1.11}$ powder samples (Al/Si ratio of 20) are presented in Fig. S2.† The weak NaAl(SO$_4$)$_2$·6H$_2$O diffraction peak appears in PSAS$_{1.11}$ at the Al molar ratio of 1/12. When the molar ratio of aluminum can be increased to 3/12, the main crystalline phase of PSAS$_{1.11}$ is sodium aluminum sulfate hexahydrate. This result indicates that the basicity of PSAS increases with the increase of aluminum molar ratio. Meanwhile, aluminum sulfate exhibits easy loss of crystalline water. PSAS is a polymeric inorganic polymer whose molecular weight increases with the degree of polymerization. Its molecular weight varies from several hundreds to hundreds of thousands.[12] Therefore, it has no long-
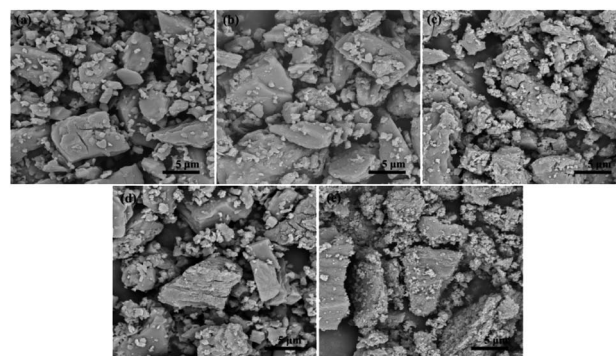

Fig. 4 SEM images of different Al molar ratio of PSAS$_{1.11}$ powder sample with an Al/Si ratio of 20, (a) 0, (b) 1/12, (c) 2/12, (d) 3/12 and (e) 4/12.

range crystalline order structure, which is consistent with other literature reported.[14]

3.3.2 PSAS$_{1.11}$ powder morphology and FTIR analysis. Fig. 4(a)–(e) shows the microscopic morphology of the PSAS$_{1.11}$ powder sample with different Al molar ratio. It is known from the figure that PSAS$_{1.11}$ coagulant is composed of irregular block. As the basicity increases, the coagulant powder sample is manifested as a dehydration, which was consistent with the XRD results.

FTIR analysis of the PSAS$_{1.11}$ powder samples with Al/Si ratio of 20 is shown in Fig. 5. Comparison with the precursor IR shows that some of the functional groups in the coagulant undergo obvious changes. The aluminosilicate skeleton peak of the alkaline intermediate located at 976 cm^{-1} was not significantly observed in the PSAS, indicating involvement of silica–aluminosols in the polymerization of the PSAS, the result that we expected. The stretching vibration of Si–O–Al bond is obvious at the peak of 948 cm^{-1}. The peaks at 603–605 cm^{-1} are associated with Si–O bonds. Peaks of 723.48 cm^{-1} and 632 cm^{-1} are the tensile and bending vibrations of Al–OH in sodium aluminate, respectively. However, this structure was not detected in PSAS, indicating that sodium aluminate was completely
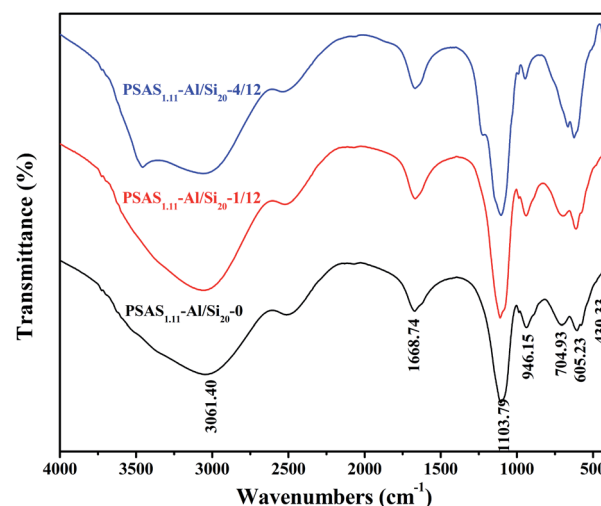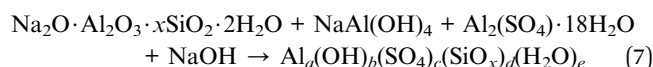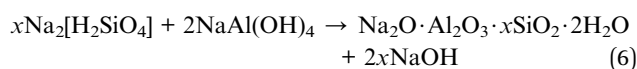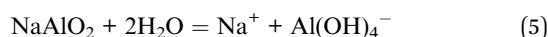
Table 2   Influence of the ratio of aluminum to silicon in PSAS$_{1.11}$ on the pH value and stability

Al/Si	25/1	20/1	15/1	12/1	10/1
pH value (PSAS$_{1.11}$)	3.11	3.15	3.24	3.29	3.31
Gel time (day)	30	20	16	14	10

Fig. 5   IR spectra of PSAS$_{1.11}$ coagulants.

Paper

involved in the polymerization reaction of PSAS. A broader peak appears at 3061 cm^{-1}, which is characteristic of the C–O–H in stabilizers.[31] The peak at 1103.79 cm^{-1} is the stretching vibration of the Al–OH–Al structure. –OH– group combined with different metal produces a slight shift in the position of the characteristic peak of this structure.[23]

3.3.3 Discussion on PSAS reaction takes place. First, sodium aluminate was mixed with a small amount of clarifying agent then dissolved in deionized water. The solution was boiled and then cooled to room temperature. The reaction occurs in this process is shown in eqn (5). The second step is the synthesis of Si–Al sol precursor. That is, sodium silicate was mixed with sodium aluminate to form an alkaline colloid. The structure of this colloid is similar to the structure of zeolite before crystallization transformation.[20] Precursor synthesis reaction is presented in eqn (6). In the third step, when the milky white solute precursor is slowly added dropwise to the aluminum sulfate solution, the solute precursor undergoes rapid dissolution and then participates in the PSAS polymerization reaction. Then, the clear aluminum sulfate solution gradually becomes translucent. After boil digesting process, the translucent PSAS solution gradually was obtained.[32,33] The reaction of the precursor with aluminum sulfate for preparing PSAS is shown in eqn (7).

$$NaAlO_2 + 2H_2O = Na^+ + Al(OH)_4^- \tag{5}$$

$$xNa_2[H_2SiO_4] + 2NaAl(OH)_4 \rightarrow Na_2O \cdot Al_2O_3 \cdot xSiO_2 \cdot 2H_2O + 2xNaOH \tag{6}$$

$$Na_2O \cdot Al_2O_3 \cdot xSiO_2 \cdot 2H_2O + NaAl(OH)_4 + Al_2(SO_4) \cdot 18H_2O + NaOH \rightarrow Al_a(OH)_b(SO_4)_c(SiO_x)_d(H_2O)_e \tag{7}$$

The molecular formula of PSAS: $Al_a(OH)_b(SO_4)_c(SiO_x)_d(H_2O)_e$, wherein, $a = 1.0$, $b = 0.75$–2.0, $c = 0.3$–1.12, $d = 0.005$–0.1, $e > 4$, $x = 2.0$–4. According to the above reactions, the schematic of preparing PSAS from the precursor is shown in Fig. 6.

3.3.4 Characteristics of Al species distribution in liquid PSAS$_{1.11}$. Based on the different reaction time of aluminum species with the Ferron reagent, the Al species in coagulant would allow divided into three types: Al_a, Al_b and Al_c. Al_a refers to the mononuclear aluminum hydroxy complex (Al^{3+}, $Al(OH)^{2+}$, $Al(OH)_2^+$ and $Al(OH)_4$) and the primary polymer ($Al_2(OH)_2^{4+}$, $Al_2(OH)_5^+$ and $Al_3(OH)_8^+$, $etc.$). The reaction of this complex with Ferron reagent is usually completed within 1 minute. Al_b stands for the polynuclear hydroxyl complex of aluminum, generally refers to the oligomers of aluminum ($Al_6(OH)_{12}^{6+}$, $Al_7(OH)_{16}^{5+}$ and $Al_8(OH)_{20}^{4+}$) and middle polymers ($Al_{13}(OH)_{32}^{7+}$, $Al_{13}O_4(OH)_{24}^{7+}$ and Al_n). This part of Al is the active ingredient of the coagulant, which usually completes its reaction with Ferron within 120 minutes. The remaining aluminum-containing part (Al_c) hardly reacts with Ferron's reagent. It's usually considered as the hydrolysis polymerized macromolecules of aluminum ($Al_{15}(OH)_{36}^{9+}$ and Al_{30}, $etc.$), colloidal molecules and precipitates ($Al(OH)_3$), $etc.$[12] The Al-Ferron timed spectrophotometric curve not only reflects the difficulty of the reaction of different aluminum species with Ferron, but also roughly reflects the polymerization degree of the coagulant.

The complex reaction of PSAS$_{1.11}$ and Ferron over time is shown in Fig. 7. With the increase of the aluminum molar ratio (precursor/aluminum sulfate), the basicity of PSAS$_{1.11}$ coagulants gradually increases. This reflects the slow complexation reaction of Al and Ferron reagents. The PSAS$_{1.11}$-0 solution showed the largest absorbance value, indicating the fastest complex reaction of Al and Ferron reagents. This result indicates that PSAS$_{1.11}$-0/12 has the most mononuclear hydroxyaluminum complexes and primary aggregates. Polynuclear hydroxyl complexes of aluminum in PSAS$_{1.11}$-1/12 and PSAS$_{1.11}$-4/12 flocculants increased significantly. Especially, the result is more obvious when the basicity of the PSAS increases to more than 50%. Table S1† presents the Al species specific distribution of examined PSAS$_{1.11}$ coagulants. Knowable, Al species in the coagulants prepared by sol method are mainly Al_a and Al_b. This result is attributable to the fact that the sol precursor first dissolves in aluminum sulfate and then polymerizes.
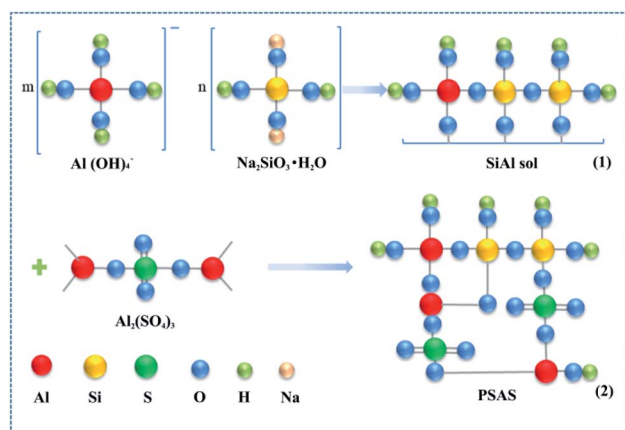

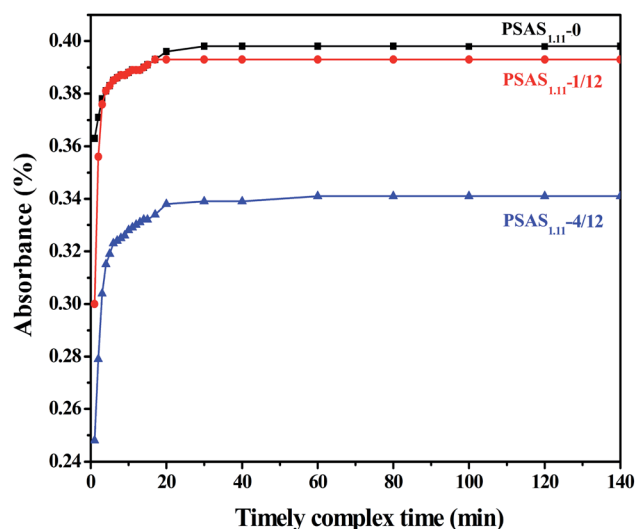
Fig. 6 Schematic synthesis of sol precursor and PSAS.

Fig. 7 Al-Ferron timed complex curve.

3.4 Decolorization performance of liquid PSAS$_{1.11}$ on Congo red dye wastewater

3.4.1 Effect of PSAS$_{1.11}$ on the decollation rate of dyeing wastewater.

The coagulation performance test of PSAS$_{1.11}$ was studied using 100 mg L^{-1} Congo red dye simulated wastewater. With coagulant dose of 4 mg L^{-1} and initial pH of 7.0, performance of PSAS$_{1.11}$ coagulants prepared with different Al molar ratio of precursor to aluminum sulfate was evaluated in Fig. 8(a). The worst decolorization rate of PSAS$_{1.11}$ prepared by the sol precursor without sodium aluminate was 74.68%. Since the precursor do not contain sodium aluminate and thus do not form silica-alumina sol, this leads to poor removal results. As Al molar ratio of precursor to aluminum sulfate increases, the basicity of PSAS$_{1.11}$ coagulant gradually increases but the silicon content gradually decreases, and its performance first increases and then decreases. The overall performance was better than that of PSAS$_{1.11}$ prepared by precursor without the addition of sodium aluminate. The results imply that the sol method is beneficial to improve coagulant performance. Meanwhile, at the given conditions, PSAS$_{1.11}$ (Al molar ratio of 12, Al/Si of 21.6) coagulant showed high coagulation performance with 87.32% color removal rate.

To clearly understand the reasons for the decline in coagulant performance, another group of PSAS$_{1.11}$ coagulant with Al/Si of 20 prepared by different Al molar ratio was used. Fig. 8(b) shows the effect of coagulants with different Al molar ratios on the decolorization of dyeing wastewater. The same trend was observed compared to the above results. From the comparison of Fig. 8(a) and (b), the performance of PSAS$_{1.11}$ (Al molar ratio of 12, Al/Si of 20) is improved, with decolorization rate of 89.9%, compared to PSAS$_{1.11}$ (Al molar ratio of 12, Al/Si of 21.6). So,
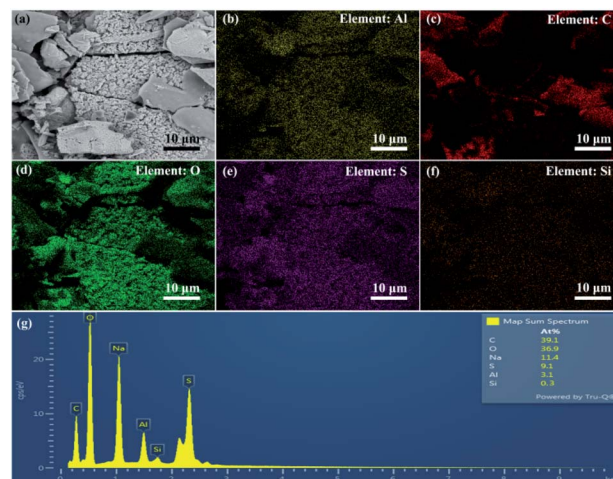

Fig. 9 Flocs (a) SEM image, (b)–(f) elemental mapping and (g) EDS pattern.

a certain degree of Al to Si ratio reduction can effectively improve the performance of coagulants. However, at the given condition (Al/Si of 20), the increase of coagulant basicity is not conducive to the decolorization of dyeing wastewater. It is not difficult to find the best performance of the PSAS coagulant prepared by using the Al molar ratio of 1/12. From the analysis of aluminum species distribution in PSAS$_{1.11}$ (Al/Si of 20), increasing the basicity of coagulant caused the increase of Al$_b$, so the performance of coagulant increased. However, when Al molar ratio is greater than 1/12, Al$_c$ increases, so the performance of coagulant shows a decreasing trend. Therefore, the suitable molar ratio of Al for the synthesis of PSAS$_{1.11}$ coagulant is 1/12.

Fig. 8(c) shows the effect of different aluminum to silicon ratio of PSAS$_{1.11}$ coagulants on the decolorization of dye wastewater. According to the performance test results, it can be seen that the decolorization ability of PSAS$_{1.11}$ increases first and then decreases as the ratio of aluminum to silicon decreases. Suitable aluminum to silicon ratio of coagulants is between 15 and 20. The smaller the Al to Si ratio, the more pronounced the colloidal material observed in the coagulant, especially at an Al to Si ratio of 10. This result leads to a decrease in coagulant performance. Summarizing, PSAS$_{1.11}$-1/12 coagulant with Al to Si ratio of 20 has the most excellent coagulation performance.

Well knows, coagulation is a physic-chemical process, which is highly dependent on solution pH, especially in the case of aluminum-based coagulants.[34,35] So, in subsequent performance tests, we focus on PSAS$_{1.11}$ (Al molar ratio of 12, Al/Si of 20) coagulant. The effects of the starting pH of the solution and the coagulant dose on the color removal rate are provided in Fig. 8(d). With below a dose of 8 mg L^{-1}, the suitable working pH of PSAS$_{1.11}$ coagulant is 9. At a relatively lower dosage of 4 mg L^{-1}, the color removal efficiency of the coagulant of PSAS$_{1.11}$ can reach 91.9%. However, with the increase of the dosage, the suitable working pH value of the coagulant increases. The suitable pH for dyeing wastewater treatment was
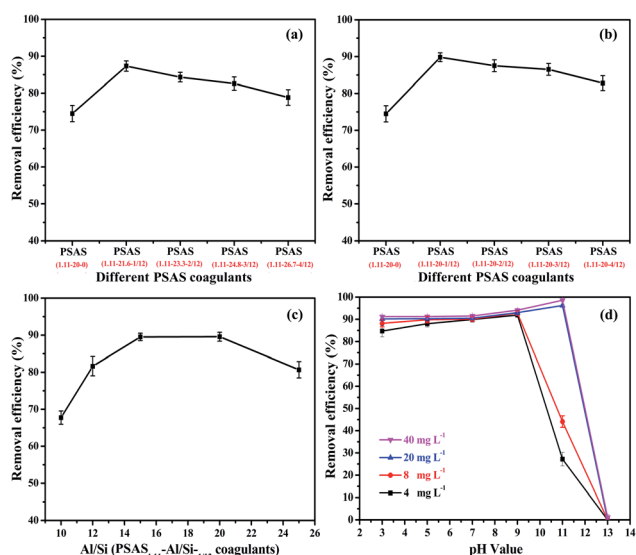

Fig. 8 (a) The effect of the coagulant with the initial ratio of Al–Si of 20 on the removal of dye wastewater, (b) effect of constant Al–Si ratio of 20 with different basic degrees on performance of coagulant, (c) the effect of aluminum–silica ratio on the performance of coagulant. (d) The effects of the solution pH and the coagulant (PSAS$_{1.11}$-1/12) dose on performance.

11 when the coagulant dose exceeded 20 mg L^{-1}. In particular, PSAS$_{1.11}$ shows excellent performance with color removal rate of 98.6% at the coagulant dosage of 40 mg L^{-1}. Moreover, the coagulation performance of PSAS$_{1.11}$ is compared against some coagulants reported references in Table S2.†[36–39] This result clearly shows that as-prepared coagulant has high coagulation performance.

Moreover, the wastewater pH treated by coagulant was measured. With coagulant dosage of 4–8 mg L^{-1} and dyeing wastewater initial pH value of 3–9, the pH of the final treated solution is less than 5.0. However, working pH of 11, the pH value of the treated solutions are all greater than 10. When the coagulant dose was increased to 20 mg L^{-1}, the pH of the treated solution decreased to below 6. Therefore, PSAS has a significant color removal rate for dyeing wastewater when the solution treated is acidic. A reasonable explanation that this result is relates to the Al species. Dissolved aluminum species Al(OH)$_4^-$ > 6.8 can lead to the diminishing of Al(OH)$_3$ precipitates,[27] resulting in lower color uptake.

3.4.2 SEM and FTIR analysis of floc. The Congo red dye wastewater was treated with PSAS$_{1.11}$ coagulant (Al molar ratio of 1/12, Al/Si of 20) and left for 24 h. After pouring off the supernatant, the residual solid–liquid mixture was vacuum dried at 50 °C for 48 h to obtain the desired flocculent. In order not to affect the floc structure analysis, flocs obtained at a lower dose of 20 mg L^{-1} and the dyeing wastewater initial pH of 11 was used to the relevant tests. The microstructure of flocculent powder was observed by SEM electron microscopy as shown in Fig. 9(a). The flocs produced by the combination of PSAS$_{1.11}$ and Congo red were mostly composed of flaky masses. This result indicates that the coagulant is tightly bound to Congo red in Fig. 9(b)–(f), resulting flocs are easy to settle.

Fig. 10 shows the FTIR spectra of Congo red dye and flocculent. Black line is the transmittance curve of Congo red. The peak at 1128.97 cm^{-1} is the characteristic peak of R–SO$_3$–

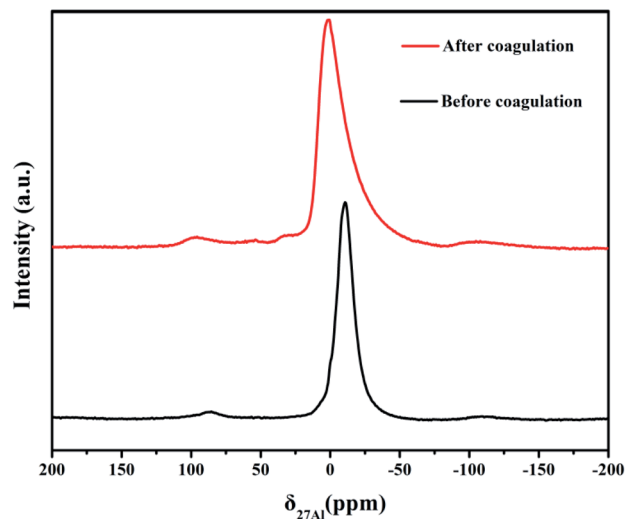**Fig. 11** ^{27}Al NMR spectra for PSAS$_{1.11}$ coagulant and floc.

structure. The peaks at 640 and 616 cm^{-1} are characteristic of C–H stretching vibrations of a disubstituted aromatic compound. After coagulant combined with the dye, the result of the infrared spectrum of the floc is shown in the red curve. Comparing the two curves, the intensity of the characteristic peak of R–SO$_3$– structure at 1128.97 cm^{-1} is significantly weakened. The two R–SO$_3$– groups were joined by Al$_a$ or Al$_b$ to form the R–SO$_3$–Al$_a$–SO$_3$–R or R–SO$_3$–Al$_b$–SO$_3$–R structures resulting in a decrease in the intensity of the characteristic peak of the R–SO$_3$– structure. Suggesting that PSAS$_{1.11}$ mainly reacts chemically with this structure, which is consistent with literature reports.[38]

3.4.3 Typical ^{27}Al NMR spectrum and Raman spectrum of PSAS$_{1.11}$ coagulant and floc. The black curve in Fig. 11 shows the type of Al in the PSAS$_{1.11}$ coagulant. A resonance signal is observed in the spectra, at the chemical shift of about 0 ppm near, which is induced by the octahedral Al$_a$ and Al$_b$. Zhang *et al.* showed that the response of Al$_{13}$ was weaker for basicity below 33.3%. This response signal gradually decreases with the increase of silicon content until it disappears.[40] So, the corresponding signal of Al$_{13}$ was not found at 63 ppm. From the red curve, it can be seen that PSAS$_{1.11}$ undergoes hydrolysis reaction in the coagulation process. Polymers of aluminum bind directly to the dye molecules thus enabling the decolorization of dye wastewater.

Fig. S4† showed the Raman spectra of PSAS$_{1.11}$ coagulant and floc. One typical feature is the result of scattering presentation of Al$_2$SO$_4$. The whole Raman spectral curve is not flat, which is caused by the no long-range crystalline order of polymers. In the red curve, the Raman shift is at 1442–1380 cm^{-1} for the –N=N– and aromatic ring conjugated structure.[41] The peak of R–O–SO$_2$– structure was found at about 1156 cm^{-1}. The results indicate that the polymer of aluminum interacts with the sulfonic acid group in Congo red. This result is consistent with FTIR.
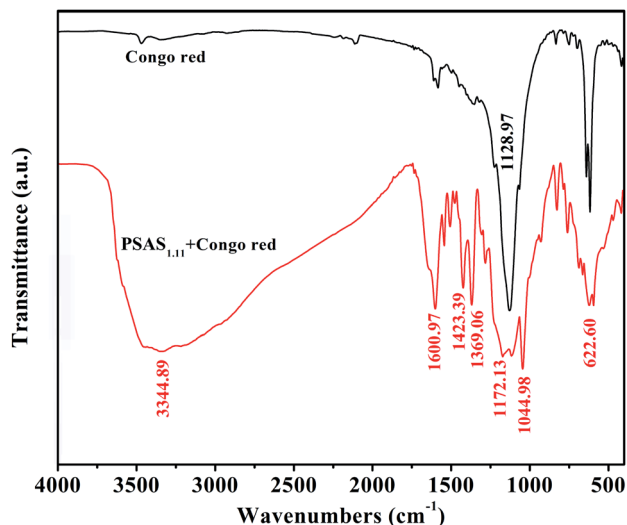

Fig. 10 FTIR spectrum of Congo red dye and floc (Congo red and PSAS$_{1.11}$).
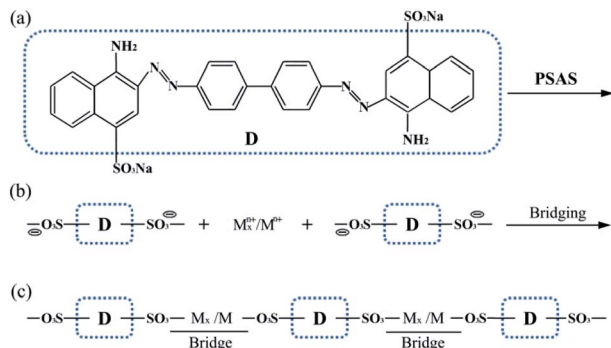
Fig. 12 Illustration of Congo red removal mechanism; (a) molecular structure of Congo red (D: subportion of Congo red without the ionizable group) and (b) charge neutralization between the anionic Congo red moiety and monomeric and polymeric metal ions (M_x^{n+}/M^{n+}); (c) interparticle bridging between Al-pollutant complexes and anion.

3.4.4 Congo red removal mechanism. Fig. 12 illustrates the decolorization mechanism of PSAS$_{1.11}$ coagulant. After dissolving in water, Congo red is easily ionized to form sodium cation and organic anion. At suitable pH, the appropriate amount of coagulant is added to the dye wastewater. In this case, Al$_a$ (Al^{3+}, Al(OH)$_2$$^+$ and Al(OH)$^{2+}$) and Al$_b$ are hydrolyzed. The hydrolysis product of Al$_a$ and Al$_b$ or Al$_a$ and Al$_b$ are directly combined with Congo red without sodium ions (Fig. 12(b)). Al$_c$ would be considered as little or almost no effect on decolorization behavior. The chemical reactions that charge neutralization occurs among anionic Congo red moiety, monomeric and polymeric metal ions are definitely happening. Two anionic Congo red moiety are bound to each other by positively charged aluminum polymer diaspora as shown in Fig. 12(c). The final coagulation process is accomplished by bridging mechanism.[38]

4. Conclusions

(1) Silica-alumina sol precursor was successfully used to synthesize poly-silicate aluminum sulfate coagulant. The prepared PSAS$_{3.27}$ coagulant exhibits poor stability and high turbidity, with significant gelation typically occurring after 2–3 days of storage at ambient temperature. This makes it unsuitable for further testing and analysis. However, the PSAS$_{1.11}$ coagulant solution prepared by low modulus (1.11) water glass had the advantages of low turbidity and good stability. With aluminum–silica ratio of 20 and the Al molar ratio (precursors to aluminum sulfate) of 3/12 or more, as-prepared PSAS$_{1.11}$ coagulant had the long-term stability, no gel for several months. Therefore, it is of obvious practical significance to carry out further research on PSAS$_{1.11}$ coagulant.

(2) Al species distribution analysis of PSAS$_{1.11}$ shown that the initial aggregation state Al (Al$_a$) is gradually changes to Al (Al$_b$ and Al$_c$) in the polymerization states and solids, with the increase of basicity.

(3) PSAS$_{1.11}$ coagulant prepared with an aluminum-silica ratio of 20 and Al molar ratio of 1/12 between precursor to aluminum sulfate had good performance for dyeing wastewater

treatment, and the color removal rate reached 98.6%, at solution initial pH of 11 and coagulant dosage of 40 mg L^{-1}.

(4) The decolorization mechanism of PSAS$_{1.11}$ coagulant suggested, charge neutralization reactions occur between the anionic Congo red molecules and the monomeric and polymeric metal ions. Two anionic Congo red molecules are bound together by positively charged aluminum polymers, thus completing the removal of the dye through a bridging process.

Author contributions

The contributions of all authors are now introduced as follows: the first author Yunlong Zhao completed the experiment and paper writing. Yajie Zheng mainly guided the paper direction and paper revision. Yinglin Peng participated in part of the experimental research and discuss. Hanbing He completed XRD and SEM data analysis. Zhaoming Sun completed part of the data analysis.

Conflicts of interest

There are no conflicts to declare.

References

1 J. Abdi, M. Vossoughi, N. M. Mahmoodi and I. Alemzadeh, Synthesis of metal-organic framework hybrid nanocomposites based on GO and CNT with high adsorption capacity for dye removal, *Chem. Eng. J.*, 2017, **326**, 1145–1158.

2 V. Katheresan, J. Kansedo and S. Y. Lau, Efficiency of various recent wastewater dye removal methods: a review, *J. Environ. Chem. Eng.*, 2018, **6**(4), 4676–4697.

3 C. R. Holkar, A. J. Jadhav, D. V. Pinjari, M. Naresh, N. M. Mahamuni and A. B. Pandit, A critical review on textile wastewater treatments: possible approaches, *J. Environ. Manage.*, 2016, **182**, 351–366.

4 Z. Z. Sun, Z. H. Liu, L. Han, D. L. Qin, G. Yang and W. H. Xing, Study on the treatment of simulated azo dye wastewater by a novel micro-electrolysis filler, *Water Sci. Technol.*, 2019, **79**(11), 2279–2288.

5 H. Zazou, H. Afanga, S. Akhouairi, H. Ouchtak, A. A. Addi, R. A. Akbour, A. Assabbane, J. Douch, A. Elmchaour, J. Duplay, A. Jada and M. Handani, Treatment of textile industry wastewater by electrocoagulation coupled with electrochemical advanced oxidation process, *J. Water. Process. Eng.*, 2019, **28**, 214–221.

6 N. Dafale, N. N. Rao, S. U. Meshram and S. R. Wate, Decolorization of azo dyes and simulated dye bath wastewater using acclimatized microbial consortium-biostimulation and halo tolerance, *Bioresour. Technol.*, 2008, **99**(7), 2552–2558.

7 H. P. Jia, H. Gang, Z. Rui and X. S. Zhao, Hierarchical N-doped TiO$_2$ hollow microspheres consisting of nanothorns with exposed anatase 101 facets, *Chem. Commun.*, 2011, **47**(24), 6942–6944.

8 H. Mittal, A. Maity and S. S. Ray, Gum karaya based hydrogel nanocomposites for the effective removal of cationic dyes from aqueous solutions, *Appl. Surf. Sci.*, 2016, **364**, 917–930.

9 H. Li, S. Liu, J. Zhao and N. Feng, Removal of reactive dyes from wastewater assisted with kaolin clay by magnesium hydroxide coagulation process, *Colloids Surf., A*, 2016, **494**(5), 222–227.

10 T. Chen, B. Gao and Q. Yue, Effect of dosing method and pH on color removal performance and floc aggregation of polyferric chloride-polyamine dual-coagulant in synthetic dyeing wastewater treatment, *Colloids Surf., A*, 2010, **355**(1–3), 121–129.

11 Y. J. Zheng, Z. Q. Gong, L. H. Liu and B. Z. Chen, Comparisons of species and coagulation effects of PFS solution and solid PFS from pyrite cinders, *T. Nonferr. Soc.*, 2002, **12**(005), 983–986.

12 H. X. Tang, *Inorganic polymer flocculation theory and coagulant*, China Building Industry Press, 2006, ch 4.

13 J. Ma, R. Wang, X. Wang, H. Zhang, B. Zhu, L. L. Lian and D. W. Lou, Drinking water treatment by stepwise flocculation using polysilicate aluminum magnesium and cationic polyacrylamide, *J. Environ. Chem. Eng.*, 2019, **7**(3), 103049.

14 T. Sun, L. L. Liu, L. L. Wan and Y. P. Zhang, Effect of silicon dose on preparation and coagulation performance of poly-ferric-aluminum–silicate-sulfate from oil shale ash, *Chem. Eng. J.*, 2010, **163**(1–2), 48–54.

15 L. L. Cai, Y. Q. Xie, Q. P. Zhuang and M. Niu, Effects of polysilicate aluminum sulfate on fire resistance of ultra-low density materials, *J. Beijing For. Univ.*, 2014, **36**(5), 136–141.

16 Z. M. Qiu, W. T. Jiang and Z. J. He, Post-treatment of banknote printing wastewater using polysilicate ferro-aluminum sulfate (PSFA), *J. Hazard. Mater.*, 2009, **166**(2–3), 740–745.

17 S. Q. Li, P. J. Zhou, D. Ling and K. Feng, Treatment of oily wastewater using composite flocculant of polysilicate ferro-aluminum sulfate – rectorite, *J. Water. Res. Prot.*, 2011, **3**(4), 253–261.

18 J. Li, T. Xu, D. J. Bao, Z. L. Xu and Z. M. Liu, Study on the flocculation performance of poly-silicate aluminum and magnesium on domestic sewage, *Appl. Mech. Mater.*, 2014, **7**, 587–589.

19 Z. M. Qiu, J. W. Tiang and Z. J. He, Post-treatment of banknote printing wastewater using polysilicate ferro-aluminum sulfate (PSFA), *J. Hazard. Mater.*, 2009, **166**(2–3), 740–745.

20 Q. Li, S. Wang and L. Wang, Disposal of Arsenic Wastewater by Polysilicate Metal Sulfates in Power Plant, *The 3rd International Conference on Bioinformatics and Biomedical Engineering (iCBBE)*, 2009, pp. 1–4.

21 J. Ma, R. Wang, X. Wang, *et al.*, Drinking water treatment by stepwise flocculation using polysilicate aluminum magnesium and cationic polyacrylamide, *J. Environ. Chem. Eng.*, 2019, **7**(3), 103049.

22 W. Zhang, T. Zhang, L. Xi, H. J. Gu, Y. H. Hu, C. Gu and Y. J. Zhang, Preparation of new type poly-silicate coagulant and its coagulation property, *Energy Procedia*, 2012, **17**(1), 1627–1634.

23 Z. Y. You, L. Zhang, S. J. Zhang, Y. J. Sun and K. J. Shah, Treatment of oil-contaminated water by modified polysilicate aluminum ferric sulfate, *Processes*, 2018, **6**(7), 95.

24 R. H. Busey and R. E. Mesmer, Ionization equilibriums of silicic acid and polysilicate formation in aqueous sodium chloride solutions to 300 °C, *Inorg. Chem.*, 1997, **16**(10), 2444–2450.

25 Y. L. Zhao, Y. J. Zheng, H. B. He, Z. M. Sun and A. Li, Silica extraction from bauxite reaction residue and synthesis water glass, *Green. Process. Synth.*, 2021, **10**, 268–283.

26 A. K. Tolkou, M. Mitrakas, I. A. Katsoyiannis, M. Ernst and A. I. Zouboulis, Fluoride removal from water by composite Al/Fe/Si/Mg pre-polymerized coagulants: characterization and application, *Chemosphere*, 2019, **231**, 528–537.

27 J. Singh and R. L. White, A variable temperature infrared spectroscopy study of NaA zeolite dehydration, *Vib. Spectrosc.*, 2017, **94**, 37–42.

28 Y. Zeng and J. Park, Characterization and coagulation performance of a novel inorganic polymer coagulant-poly-zinc-silicate-sulfate, *Colloids Surf, A*, 2009, **334**(1–3), 147–154.

29 D. Hasse, N. Spiratos and C. Jolicoeur, *European Patent*, no. 0372715A1, 1990, vol. 6, p. 13.

30 W. Stumm, H. Huper and R. L. Champlin, Formulation of polysilicates as determined by coagulation effects, *Enviorn. Sci. Technol.*, 1967, **1**(3), 221–227.

31 Q. Lin, H. Peng, S. Zhong and J. X. Xiang, Synthesis, characterization, and secondary sludge dewatering performance of a novel combined silicon–aluminum–iron–starch flocculant, *J. Hazard. Mater.*, 2015, **285**, 199–206.

32 W. Liu, Z. L. Yin and Z. Y. Ding, Low-temperature phase transitions of sodium aluminate solutions, *T. Nonferr. Soc.*, 2019, **29**, 194–199.

33 H. Wang, Q. M. Feng and K. Liu, The dissolution behavior and mechanism of kaolinite in alkali-acid leaching process, *Appl. Clay Sci.*, 2016, **132–133**, 273–280.

34 S. Aoudj, N. Drouiche, M. Hecini, T. Ouslimane and B. Palaouane, Coagulation as a post-treatment method for the defluoridation of photovoltaic cell manufacturing wastewater, *Proc. Eng.*, 2012, **33**, 111–120.

35 Z. He, R. Liu, Z. Hu, H. Liu and J. Qu, Defluoridation by Al-based coagulation and adsorption: species transformation of aluminum and fluoride, *Separ. Purif. Technol.*, 2015, **148**, 68–75.

36 K. Prajapati, L. G. Sorokhaibam, V. M. Bhandari, D. J. Killedar and V. V. Ranade, Differentiating process performance of various coagulants in removal of Congo Red and Orange G Dyes, *Int. J. Chem. React. Eng.*, 2016, **14**(1), 195–211.

37 H. Patel and R. T. Vashi, Removal of Congo Red dye from its aqueous solution using natural coagulants, *J. Saudi Chem. Soc.*, 2012, **16**(2), 131–136.

38 Y. X. Wei, Q. Z. Ji, L. Chen, J. W. Hao, C. L. Yao and X. Z. Dong, Preparation of an inorganic coagulant-polysilicate–magnesium for dyeing wastewater treatment: effect of acid medium on the characterization and coagulation performance, *J. Taiwan. Inst. Chem.*, 2017, **72**, 142–148.

39 J. Garvasis, A. R. Prasad, K. O. Shamsheera, P. K. Jaseela and A. Joseph, Efficient removal of Congo red from aqueous solutions using phytogenic aluminum sulfate nano coagulant, *Mater. Chem. Phys.*, 2020, **251**, 123040.

40 P. Zhang, H. Hahn, E. Hoffmann, E. Hoffmann and G. Zeng, Influence of some additives to aluminium species distribution in aluminium coagulants, *Chemosphere*, 2004, **57**(10), 1489–1494.

41 J. A. Dean, *Lang's Handbook of Chemistry*, Science Press, Beijing, 15th edn, 2003, ISBN: 7-03-010409-9.05.